Generalized Model-Free Analysis of Nuclear Spin Relaxation Experiments

Xiaolin Xu[1], Andrey V. Struts[1,2] & Michael F. Brown[1]

[1] *University of Arizona, Tucson, AZ, USA*
[2] *St. Petersburg State University, St. Petersburg, Russia*

NMR spectroscopy is one of the most widely used experimental tools in chemistry and physics. Compared with methods such as X-ray crystallography, both structural and dynamical information is obtained. The analytic formulations in NMR spectroscopy are complementary to numerical molecular dynamics (MD) simulations in terms of theoretical force fields based on experimental data. Generalized model-free (GMF) analysis bridges theory and experiment by introducing an irreducible representation of the nuclear spin interactions (dipolar and quadrupolar coupling and chemical shift), which transforms under rotations by the Wigner rotation matrix. Solid-state NMR experiments characterize the dynamical variables by including the amplitudes and rates of motions within the alignment frame, e.g., crystal axes system, or director frame for liquid crystals or biomembranes. According to time-dependent perturbation theory, the NMR relaxation rates depend on the spectral densities of motion due to the irreducible components of the coupling Hamiltonian. The mean-squared amplitudes and correlation times together with the activation barriers characterize the structural dynamics. Application to rhodopsin gives an example where the methyl groups of the retinal cofactor have different motional rates and activation barriers that change with light activation. The simple framework of GMF analysis can be applied to relaxation experiments for various biomolecular systems, including membrane proteins, amyloid fibrils, and aligned biopolymers.

Keywords: coupling interactions, deuterium NMR, GMF analysis, GPCR, membrane proteins, residual quadrupolar coupling, rhodopsin

How to cite this article:
eMagRes, 2014, Vol 3: 275–286. DOI 10.1002/9780470034590.emrstm1367

Introduction

In NMR spectroscopy, the experimental line shapes are related to molecular structures, whereas the nuclear spin relaxation rates characterize the dynamics (see Amphiphilic Liquid Crystalline Samples: Nuclear Spin Relaxation, Deuteron Relaxation Rates in Liquid Crystalline Samples: Experimental Methods, Liquid Crystalline Samples: Relaxation Mechanisms, and Relaxation Studies of Solid Biopolymers).[1−3] The origin of the nuclear spin relaxation is due to the fluctuations of the molecules about their average structures.[4] Within the broad context of molecular spectroscopy, the Hamiltonian operator $\widehat{H}(t)$ describes how the system evolves with time. It depends on both spatial and spin coordinates, and its expectation value corresponds to the spectral line frequencies. When molecular motions are present, as for flexible (bio) molecules, the equilibrium structure involves the residual Hamiltonian $\langle\widehat{H}\rangle$ averaged over the spatial coordinates.[5] The angular brackets denote a time or ensemble average in accord with the ergodic principle, where the spectral line shape corresponds to the expectation value of $\langle\widehat{H}\rangle$ and thus to the average structure. Fluctuations of $\widehat{H}(t)$ about the average $\langle\widehat{H}\rangle$ give rise to the nuclear spin relaxation, which depends on the amplitudes and rates of the motions within the alignment frame (e.g., corresponding to the crystal lattice for molecular solids, or director axis for complex fluids). The mean-squared amplitudes are derived from the matrix elements of $\langle\widehat{H}(t)^2\rangle - \langle\widehat{H}\rangle^2$ due to the geometrical fluctuations about the averaged structure. Notably, the corresponding motional rates contain information about the molecular dynamics (MD). Together the structure and dynamics manifest the potentials and associated force fields that describe the properties of the system.

In this section, we describe a generalized model-free (GMF) method for interpreting experimental solid-state NMR spectra combined with the nuclear spin relaxation rates.[6,7] We show that the GMF method can be used to successfully extract both structural and dynamical information from the experimental line shapes and relaxation times. It represents a minimalist approach to obtain the mean-square amplitudes and rates of the geometrical fluctuations. A stationary Markov process is considered for the motions that give rise to the relaxation, which can be expanded upon in more detailed theoretical treatments. The analysis allows one to investigate the structure and dynamics of the system. Rhodopsin is introduced as a biophysical example, where the retinal cofactor plays a key role in initiating the visual process.[8] By probing the local dynamics of retinal using the GMF method, we can address how the cofactor affects the large-scale protein motions in the functional mechanism.[9] Knowledge of the system is acquired

that cannot readily be obtained with other physical methods such as X-ray crystallography.

Representation of Coupling Interactions in Magnetic Resonance Spectroscopy

The Hamiltonian operator $\widehat{H}$ for the nuclear interactions is closely related to the time evolution of the system of nuclear spins.[10] In the presence of an external magnetic field, it can be expressed as

$$\widehat{H}(t) = \widehat{H}_Z + \widehat{H}_\lambda(t) \tag{1}$$

where $\widehat{H}_Z$ represents the Zeeman effect due to interaction of the nuclear magnetic moment with the $\mathbf{B}_0$ field, and $\widehat{H}_\lambda$ is the perturbing Hamiltonian due to electrical or magnetic interactions of the nucleus.[1,2] The interactions of interest are the chemical shift ($\lambda \equiv$ CS), magnetic dipole–dipole interaction ($\lambda \equiv$ D), or electric quadrupole interaction ($\lambda \equiv$ Q) (see Internal Spin Interactions and Rotations in Solids and Bilayer Membranes: Deuterium and Carbon-13 NMR).[3,11] In Figure 1, we show the energy levels for a spin $I = 1$ system, together with the perturbing quadrupolar interaction and the spectral line frequencies, as an illustration. Notably, the representation of the Hamiltonian operators in equation (1) depends on the choice of basis. For many physical problems, a Cartesian basis is appropriate. However, in what follows, we change from a Cartesian to a spherical basis, which is most useful for problems involving rotational dynamics.[12]

Change of Basis – Irreducible Representation

Because the Zeeman Hamiltonian $\widehat{H}_Z$ corresponds to a scalar interaction (rank = 0), it has the same form irrespective of the basis. Evaluation of the time-independent Schrödinger equation is straightforward, using $\widehat{H}_Z = -\gamma\hbar B_0 \widehat{I}_z$ together with the eigenvalue equations for the angular momentum operators (see below). For the perturbing Hamiltonian $\widehat{H}_\lambda$ either $\lambda =$ CS (rank = 0, 1, 2) or $\lambda =$ D, Q (rank = 2) interactions are considered. We introduce a spherical basis, which is useful in the treatment of rotational motions.[3] The coupling (rank = 2) can then be expressed as the scalar product,[1,2,13]

$$\widehat{H}_\lambda = \hbar C_\lambda \widehat{\mathbf{T}} \cdot \mathbf{V} = \hbar C_\lambda \sum_{m=-2}^{2} (-1)^m \widehat{T}^{(2)\text{lab}}_{-m} V^{(2)\text{lab}}_m \tag{2}$$

which describes the nuclear interaction ($\lambda =$ D, Q). According to equation (2), the Hamiltonian $\widehat{H}_\lambda$ depends on both spin and spatial (geometric) coordinates. Here $\widehat{T}^{(2)}_m$ and $V^{(2)}_m$ are second-rank irreducible (spherical) tensors that are constructed from the components of the angular momentum operators and the coupling tensor, respectively.[12] Note that the $\widehat{T}^{(2)}_m$ operators are defined in the laboratory (lab) frame, whereas the coupling tensor $V^{(2)}_m$ is a molecule-fixed quantity that must be transformed to the laboratory axes in equation (2).

Now in the presence of an external magnetic field $\mathbf{B}_0$, the axis of quantization for the spin angular momentum is the B_z-direction. The angular momentum is quantized in the laboratory frame of $\mathbf{B}_0$ and the second-rank irreducible components are

$$\widehat{T}^{(2)\text{lab}}_0 = \frac{1}{\sqrt{6}}(3\widehat{I}_z\widehat{S}_z - \widehat{\mathbf{I}} \cdot \widehat{\mathbf{S}}) \tag{3}$$

$$\widehat{T}^{(2)\text{lab}}_{\pm 1} = \mp\frac{1}{2}(\widehat{I}_z\widehat{S}_\pm + \widehat{I}_\pm\widehat{S}_z) \tag{4}$$

$$\widehat{T}^{(2)\text{lab}}_{\pm 2} = \frac{1}{2}\widehat{I}_\pm\widehat{S}_\pm \tag{5}$$

For the electric quadrupolar coupling and homonuclear magnetic dipolar coupling $\mathbf{I} = \mathbf{S}$, and for the heteronuclear dipolar coupling $\widehat{\mathbf{I}} \neq \widehat{\mathbf{S}}$. In magnetic resonance $\widehat{\mathbf{I}} = \widehat{\mathbf{J}}/\hbar$, which corresponds to the angular momentum operator in $\hbar$ units. Accordingly, the raising and lowering operators are denoted by $\widehat{I}_\pm \equiv \widehat{I}_x \pm i\widehat{I}_y$, and similarly for $\widehat{S}_\pm$. The angular momentum operators obey the familiar commutation relations $[\widehat{I}_x, \widehat{I}_z] \neq 0$, $[\widehat{I}_y, \widehat{I}_z] \neq 0$, and $[\widehat{S}_i, \widehat{I}_i] = 0$ where $i = x, y, z$. Hence, the secular part ($m = 0$) of the perturbing Hamiltonian commutes with the Zeeman Hamiltonian and affects the NMR lineshape. The nonsecular terms ($m = \pm 1, \pm 2$) govern transitions between the spin energy levels, and give rise to the relaxation (see below).

On the other hand, the irreducible components of the coupling tensor are expressed in the principal axis system (PAS) of the molecule, and are related to the Cartesian components by[1,2]

$$V^{(2)\text{PAS}}_0 = \sqrt{\frac{3}{2}}\delta_\lambda \tag{6}$$

$$V^{(2)\text{PAS}}_{\pm 1} = 0 \tag{7}$$

$$V^{(2)\text{PAS}}_{\pm 2} = -\frac{1}{2}\delta_\lambda\eta_\lambda \tag{8}$$

Note that the largest principal value is $\delta_\lambda \equiv V^{\text{PAS}}_{zz}$ and that the asymmetry parameter is given by $\eta_\lambda \equiv (V^{\text{PAS}}_{yy} - V^{\text{PAS}}_{xx})/V^{\text{PAS}}_{zz}$. When motions occur that are faster than the inverse of the coupling parameters (in frequency units), the Hamiltonian operator in equation (2) is averaged over the spatial coordinates.

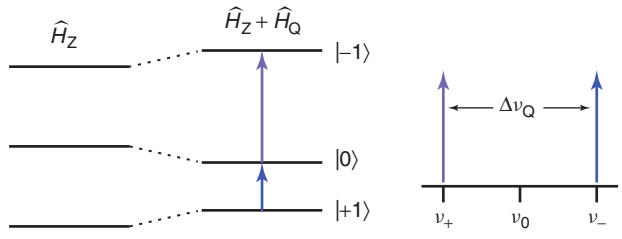

Figure 1. Example of energy levels of spin $I = 1$ system due to the Zeeman interaction together with perturbing quadrupolar interaction. The Zeeman Hamiltonian $\widehat{H}_Z$ is due to coupling of the nuclear magnetic moment to the external magnetic field $\mathbf{B}_0$, and corresponds to the unperturbed Larmor frequency ν_0. The quadrupolar coupling ($\widehat{H}_Q$) derives from the interaction of the nonspherical nuclear charge distribution with the surrounding electric field gradient. For a spin-1 system, the degeneracy of the two single-quantum transitions is removed, giving two symmetric lines at frequencies ν_+ and ν_- about the central frequency

Consequently, it is denoted by $\langle \widehat{H}_Q \rangle$ with coupling parameters $\langle V_m^{(2)\text{lab}} \rangle$ analogous to equations (6)–(8), where the angular brackets denote a time or ensemble average.

Transformation Under Rotations

In what follows, we use ^{2}H NMR spectroscopy to illuminate the general principles of our GMF approach. The quadrupolar coupling ($\lambda = Q$) is the largest of the interactions that perturb the Zeeman Hamiltonian.[14] Consequently, we consider the quadrupolar interaction for an $I = 1$ nucleus, where $C_Q \equiv eQ/2\hbar$ is the scalar factor and $\delta_Q \equiv eq$ is the largest Cartesian principal component (see Membranes: Deuterium NMR). To represent the quadrupolar Hamiltonian $\widehat{H}_Q$, we require that the components of both the spin angular momentum operators and quadrupolar coupling tensors are expressed in the laboratory frame, see equation (2). Transformation of the irreducible coupling tensor components from the molecule-fixed PAS frame into the laboratory axis system is rendered straightforward in a spherical basis, by employing the Wigner rotation matrix[12] as shown below:

$$V_m^{(2)\text{lab}} = \sum_{n=-2}^{2} V_n^{(2)\text{PAS}} D_{nm}^{(2)}(\Omega_{\text{PL}}) \tag{9}$$

The Wigner rotation matrix elements are related to the more familiar spherical harmonics by

$$\begin{aligned} D_{m0}^{(l)}(\alpha, \beta, 0) &= \sqrt{\frac{4\pi}{2l+1}} Y_{lm}^*(\beta, \alpha) \\ &= (-1)^m \sqrt{\frac{(l-m)!}{(l+m)!}} P_l^m(\cos\beta) e^{-im\alpha} \end{aligned} \tag{10}$$

where $P_l^m(x)$ are the associated Legendre polynomials with $x \equiv \cos\beta$. The Euler angles $\Omega \equiv (\alpha, \beta, \gamma)$ are illustrated in Figure 2(a). Moreover, in Figure 3, we show how the Euler angles are used in multiple frame transformations by employing rhodopsin as an example (as further explained below).

Recall that in the angular momentum representation of $|I, m\rangle$, we have $\widehat{I}^2|I, m\rangle = I(I+1)|I, m\rangle$ and $\widehat{I}_z|I, m\rangle = m|I, m\rangle$ for the eigenvalue equations, where the Dirac bra–ket notation is introduced.[10] The raising or lowering operators act upon $|I, m\rangle$ giving $\widehat{I}_\pm|I, m\rangle = \sqrt{I(I+1) - m(m \pm 1)}|I, m \pm 1\rangle$ as the result. In what follows, the vector model for angular momentum is utilized as depicted in Figure 2(b) (see below). With use of these formulas, we can readily evaluate the Hamiltonian $\widehat{H}_Z = -\gamma\hbar B_0 \widehat{I}_z$ for the Zeeman interaction, and $H_Q = \hbar C_Q \widehat{\mathbf{T}} \cdot \mathbf{V}$ for the perturbing quadrupolar interaction. Solving the time-independent Schrödinger equation, we obtain the following energy levels for the stationary states of the system:

$$E_{+1} = -\gamma\hbar B_0 + \frac{e^2qQ}{4} D_{00}^{(2)}(\Omega_{\text{PL}}) \tag{11}$$

$$E_0 = -\frac{e^2qQ}{2} D_{00}^{(2)}(\Omega_{\text{PL}}) \tag{12}$$

$$E_{-1} = \gamma\hbar B_0 + \frac{e^2qQ}{4} D_{00}^{(2)}(\Omega_{\text{PL}}) \tag{13}$$

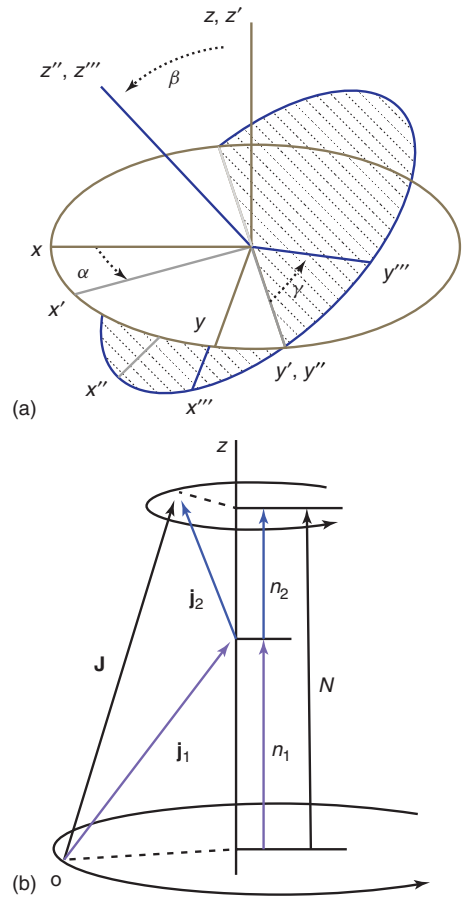

Figure 2. Illustration of how observables from solid-state NMR spectroscopy are interpreted using angular momentum theory. (a) Euler angles describe transformations of coordinate frames and simplify the treatment of nuclear spin coupling interactions. Geometrical frame transformations are carried out using Euler angle rotations where $\Omega \equiv (\alpha, \beta, \gamma)$, e.g., the principal axis system to laboratory frame. The transformation involves three consecutive rotations with two intermediate frames:[12] a primed frame (x', y', z') and a double-primed frame (x'', y'', z''). The first step is rotation of the initial frame about its own z-axis through the angle α to the primed frame. Next, we rotate the primed frame about its own y'-axis through the angle β, yielding the double-primed frame. Last, we rotate the double-primed frame about the z''-axis through the angle γ ending up with the final (laboratory) frame. Notice the line of nodes extending along the y', y'' axes. (b) Angular momentum theory underlies the analysis of nuclear spin relaxation data in NMR spectroscopy. The semi-classical vector model illustrates the coupling of two angular momenta $\mathbf{j}_1$ and $\mathbf{j}_2$ with projections n_1 and n_2 onto the z-axis to give the total angular momentum $\mathbf{J}$. The final state is specified by quantum numbers (J, N) for the total angular momentum. Note that the cone of possible orientations of $\mathbf{j}_1$ is inverted with respect to the orientation of $\mathbf{j}_2$ to illustrate the vector addition. The projection of the total angular momentum onto the z-axis is $N = n_1 + n_2$ which is quantized in $\hbar$ units. Upper and lower bounds of $|j_1 - j_2| \le J \le j_1 + j_2$ correspond to the so-called triangle $\Delta(j_1 j_2 J)$ condition. The triangle with sides $\mathbf{j}_1$, $\mathbf{j}_2$, and $\mathbf{J}$ is illustrated in the figure (see text). The uncoupled representation of angular momenta $|j_1 j_2 n_1 n_2\rangle$ is related to the coupled representation $|j_1 j_2 JN\rangle$ in terms of the vector coupling coefficients $\langle j_1 j_2 JN | j_1 j_2 n_1 n_2 \rangle$ (also known as Clebsch–Gordan coefficients). The contributions (squared coefficients) of the various coupled states (J, N) to the uncoupled states with quantum numbers $(j_1, j_2, n_1\ n_2)$ are given by $|\langle j_1 j_2 JN | j_1 j_2 n_1 n_2 \rangle|^2$. The Clebsch–Gordan series accounts for the products of the Wigner rotation matrix elements in terms of the second- and fourth-rank order parameters $\langle P_2 \rangle$ and $\langle P_4 \rangle$ (see text)

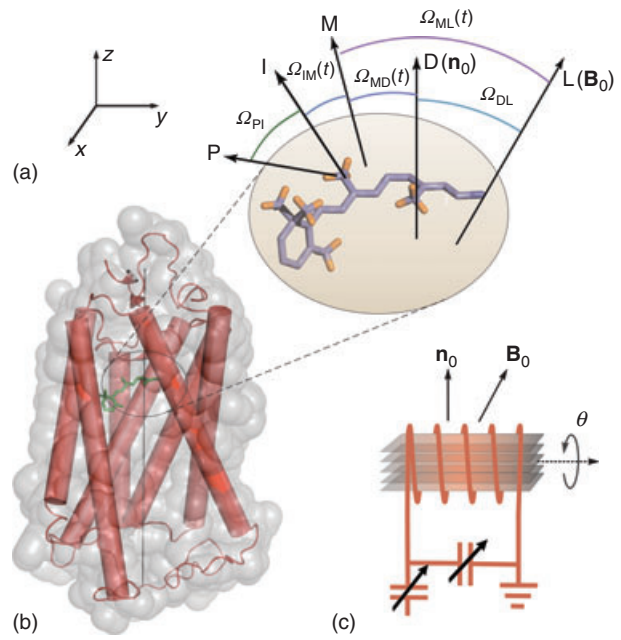

Figure 3. Membrane protein rhodopsin gives an illustrative example of the role of coordinate transformations in solid-state NMR spectroscopy. Transmembrane helices H1–H7 are shown as red rods. Euler angles used for the frame transformations are indicated by Ω_{ij} where $\{i, j\}$ denotes {P, I, M, D, L}, corresponding to the principal axis system (P), intermediate (I), molecular (M), alignment (D), and laboratory frames (L). The *z*-axes of the various coordinate frames are shown explicitly. (c) Oriented-sample NMR experiments for rhodopsin in lipid membranes are done with the alignment *z*-axis (membrane normal, $\mathbf{n}_0$) tilted at an arbitrary angle θ with respect to the magnetic field ($\mathbf{B}_0$) direction. The Cartesian coordinate frame and the aligned sample contained within the radiofrequency coil of the spectrometer are shown. (Adapted from Ref. 15. © Elsevier, 2007)

The aforementioned energy levels are obtained under the assumption of axial symmetry of the electric field gradient tensor about the C–^{2}H bond axis ($\eta_Q = 0$).

Because of the single-quantum selection rule ($\Delta m = \pm 1$), the frequencies for the resonant NMR absorptions are obtained as follows:[3]

$$\nu_+ = -\frac{\gamma}{2\pi}B_0 - \frac{3}{4}\chi_Q D_{00}^{(2)}(\Omega_{PL}) \tag{14}$$

$$\nu_- = -\frac{\gamma}{2\pi}B_0 + \frac{3}{4}\chi_Q D_{00}^{(2)}(\Omega_{PL}) \tag{15}$$

where $\chi_Q = e^2qQ/h$ is the static quadrupolar coupling constant. We can clearly see that the frequencies of the two single-quantum NMR spectral transitions are centered about the Larmor frequency $\nu_0 = -\gamma B_0/2\pi$. The chemical shift is a much smaller perturbation, and thus it is neglected. Instead of absolute transition frequencies, in solid-state ^{2}H NMR, we focus on the quadrupolar splitting,[3]

$$\Delta\nu_Q = \nu_- - \nu_+ = \frac{3}{2}\chi_Q D_{00}^{(2)}(\Omega_{PL}) \tag{16}$$

which is related to the quadrupolar coupling constant χ_Q as well as the Wigner rotation matrix for the PAS to the laboratory frame transformation.

When motions are present, the static splitting is averaged to a residual quadrupolar coupling (RQC),

$$\Delta\nu_Q = \frac{3}{2}\chi_Q\langle D_{00}^{(2)}(\Omega_{PL})\rangle \tag{17}$$

where the brackets denote a time or ensemble average as mentioned earlier. For molecules with multiple degrees of freedom, it is often desirable to decompose the overall transformation into a sequence of partial transformations using the convenient closure property of the rotation matrix:[12]

$$D_{00}^{(2)}(\Omega_{PL}, t) = \sum_{r,p,q} D_{0r}^{(2)}(\Omega_{PI})D_{rp}^{(2)}(\Omega_{IM}, t)D_{pq}^{(2)}(\Omega_{MD}, t)D_{q0}^{(2)}(\Omega_{DL}) \tag{18}$$

Applying closure to the rotation matrix element for two successive rotations, we have $D_{00}^{(2)}(\Omega_{PL}) = \Sigma_n D_{0n}^{(2)}(\Omega_{PD})D_{n0}^{(2)}(\Omega_{DL})$ which leads us to the following expression:

$$\begin{aligned}\langle D_{00}^{(2)}(\Omega_{PL})\rangle &= \sum_n \langle D_{0n}^{(2)}(\Omega_{PD})D_{n0}^{(2)}(\Omega_{DL})\rangle \\ &= \langle D_{00}^{(2)}(\Omega_{PD})\rangle D_{00}^{(2)}(\Omega_{DL})\end{aligned} \tag{19}$$

The summation has only one value of $n = 0$ because of the rotational symmetry about a preferred direction. Inserting equation (19) into equation (17) yields the result for the averaged quadrupolar splitting:

$$\Delta\nu_Q = \frac{3}{2}\chi_Q\langle D_{00}^{(2)}(\Omega_{PD})\rangle D_{00}^{(2)}(\Omega_{DL}) = \frac{3}{2}\chi_Q S_{CD} D_{00}^{(2)}(\Omega_{DL}) \tag{20}$$

The symbol $S_{CD} = \langle D_{00}^{(2)}(\Omega_{PD})\rangle$ stands for the C–D(^{2}H) segmental order parameter as a quantitative measure of the molecular or segmental flexibility, together with the average orientation. Note that in equation (20), the prefactor $\chi_Q\langle D_{00}^{(2)}(\Omega_{PD})\rangle$ can be interpreted as $\langle\chi_Q\rangle$, which is the residual (pre-averaged) quadrupolar coupling constant. Equation (20) is then completely isomorphous to equation (16), where the static coupling constant χ_Q is replaced by the residual coupling constant $\langle\chi_Q\rangle \sim \langle V_0^{(2)}\rangle$.

To illustrate the applicability to biomolecules, Figure 3 shows the case of rhodopsin (discussed subsequently).[15] Multiple frame transformations indicating the *z*-axes are shown for the retinal cofactor of rhodopsin embedded in a membrane lipid bilayer. Examples of RQCs in solid-state ^{2}H NMR spectra of rhodopsin are illustrated in Figure 4. Results are shown for three of the methyl groups of the retinal cofactor of the protein rhodopsin. Rotation of the methyl groups averages the static EFG tensor to a residual coupling tensor, whose largest principal value is projected onto the C–C^{2}H$_3$ bond axis. The motional averaging effects of methyl group rotation are shown in Figure 4, where the rates of methyl rotation vary with temperature, as discussed in the following sections.

Time-Dependent Perturbation Theory Applied to Nuclear Spin Relaxation

Now in molecular solids, as well as liquid crystals and complex fluids, the molecules are undergoing all kinds of motions. Consequently, the experimental results are the motion-averaged

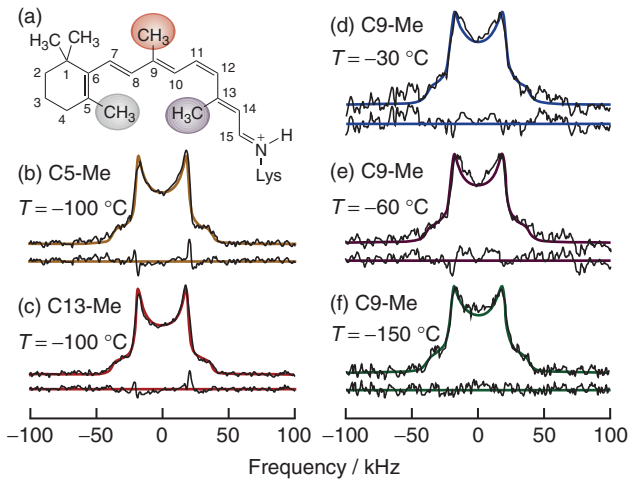

Figure 4. Solid-state ^{2}H NMR spectra for methyl groups at the C5, C9, and C13 carbons of the retinal cofactor of rhodopsin indicate rapid spinning with large off-axial order parameters. Effects of motional averaging are shown by the reduction of the static quadrupolar coupling constant χ_Q (167 kHz) to the residual quadrupolar coupling constant χ_Q (50.7–52 kHz) due to methyl rotation. (a) Chemical structure of retinal with specifically deuterated C5-, C9-, and C13-methyl groups indicated by filled circles. (b, c) Examples of solid-state ^{2}H NMR lineshapes for C5- and C13-methyl groups at −100 °C. (d–f) Solid-state ^{2}H NMR lineshapes for C9-methyl position of retinal at different temperatures. The residual quadrupolar couplings (RQCs) indicate motional averaging due to the threefold rotation of methyl groups. The off-axis motion is detected by the order parameter of the threefold axis, and varies little with temperature over the range studied. (Adapted from Ref. 15. © Elsevier, 2007)

quantities instead of their static values. The molecular motions about their average structures are the cause of the NMR relaxation. The relaxation is due to the fluctuations of the molecule-fixed coupling tensor with respect to the laboratory frame, see equation (9). A time-dependent perturbation occurs that depends on both the amplitudes and rates of the motions.[2] To evaluate the effects of the quadrupolar Hamiltonian, we apply time-dependent perturbation theory.[10] Both the motion amplitudes and rates are considered within the alignment frame, e.g., crystal frame for molecular solids, director frame for liquid crystals, fiber axis for (bio)polymers, or lipid bilayer in the case of biomembranes. The transition probabilities for the nuclear spin states are obtained by evaluating the matrix elements of the fluctuating part of the coupling Hamiltonian, leading to the results summarized in the following section.

Dynamical Information – Correlation Functions and Relaxation

As mentioned earlier, the Hamiltonian operator for the fluctuating part of the quadrupolar coupling is (see Average Hamiltonian Theory)[6]

$$\widehat{H}'_{\mathrm{Q}}(t) = \widehat{H}_{\mathrm{Q}}(t) - \langle \widehat{H}_{\mathrm{Q}} \rangle \tag{21}$$

The angular brackets $\langle \ldots \rangle$ denote a time or ensemble average over the spatial coordinates only, and are not to be confused with the quantum mechanical expectation value. In a spherical basis, the Hamiltonian is represented by equation (2) with $\lambda = \mathrm{Q}$. Because the magnetic field direction is the z-axis of quantization for the angular momentum operators, the time dependence originates from the fluctuations of the molecule-fixed coupling tensor within the laboratory coordinate frame. Examples of a sequence of transformations to the laboratory frame are shown in Figure 3(b).[15] In terms of spatial averages, the correlation functions for the irreducible components of the coupling tensor can be written as (see Brownian Motion and Correlation Times)

$$G_m(t) = \frac{\langle [V_m^{(2)\mathrm{lab}}(0) - \langle V_m^{(2)\mathrm{lab}} \rangle]^* [V_m^{(2)\mathrm{lab}}(t) - \langle V_m^{(2)\mathrm{lab}} \rangle] \rangle}{|\langle V_0^{(2)\mathrm{PAS}} \rangle|^2} \tag{22}$$

The irreducible correlation functions appear by evaluating the transition matrix elements of the nonsecular part ($m = \pm 1, \pm 2$) of the coupling Hamiltonian (see above) using time-dependent perturbation theory.[10] They are introduced at this point to show the mathematical correspondence to the physical fluctuations.

Relaxation Rates – Spectral Densities of Motion

The origin of the nuclear relaxation entails matching the power spectrum of the stochastic fluctuations at the resonance frequency to the energy gap for the spin transitions, leading to nonradiative decay from the excited state. Fourier transformation of the irreducible correlation functions gives the corresponding spectral densities. They describe the amplitudes and rates of the fluctuations of the coupling tensor components:

$$J_m(\omega) = \int_{-\infty}^{\infty} G_m(t) \mathrm{e}^{-i\omega t} \mathrm{d}t \tag{23}$$

On the basis of the theory of Alfred Redfield, upon evaluating the appropriate matrix elements, the relationships between the relaxation rates and spectral densities are (see Relaxation Theory: Density Matrix Formulation, Relaxation Theory for Quadrupolar Nuclei)[16]

$$R_{1\mathrm{Z}} \equiv \frac{1}{T_{1\mathrm{Z}}} = \frac{3}{4}\pi^2 \chi_{\mathrm{Q}}^2 [J_1(\omega_0) + 4J_2(2\omega_0)] \tag{24}$$

$$R_{1\mathrm{Q}} \equiv \frac{1}{T_{1\mathrm{Q}}} = \frac{9}{4}\pi^2 \chi_{\mathrm{Q}}^2 J_1(\omega_0) \tag{25}$$

In the aforementioned formulas, $T_{1\mathrm{Z}}$ stands for spin–lattice relaxation time, and $T_{1\mathrm{Q}}$ for the quadrupolar relaxation time, where $R_{1\mathrm{Z}}$ and $R_{1\mathrm{Q}}$ are the corresponding relaxation rates.

According to the linear combinations in equations (24) and (25), by conducting both $T_{1\mathrm{Z}}$ and $T_{1\mathrm{Q}}$ relaxation time experiments, we can directly measure the irreducible spectral densities of motion. From the vantage point of Redfield theory, the spectral densities are the primary experimental observables. They correspond to the irreducible correlation functions of equation (22) in terms of the structural and dynamical quantities that characterize the system. The Fourier transform partners directly relate the experimental observables in NMR spectroscopy to physical parameters, making it possible to study the properties of the system in terms of the underlying potential functions and force fields.

Generalized Model-Free Analysis of Solid-State NMR Relaxation Rates

Next, we need to come up with an approach to interpret the experimental data in terms of structural and dynamical information. The GMF method is broadly applicable, yet it is simple and fits the experimental data very well. It entails an irreducible representation of the coupling interaction within a spherical basis set (see above). The main assumption is that a stationary Markov process is considered for the fluctuating irreducible components relative to their averages. The resulting model-free parameter values can guide the choice of more detailed models for the MD. As a rule, the relaxation depends on the mean-squared amplitudes and correlation times for the Wigner rotation matrix elements, together with the orientation of the alignment frame (crystal lattice or director for complex fluids; bilayer normal for membrane lipids; and fiber axis for biopolymers) to the magnetic field direction (laboratory frame). The fixed transformation between the alignment frame and laboratory frame is set by the experimenter. Consequently, we are interested in the correlation functions and spectral densities that describe the structure and dynamics of the molecules within the alignment frame, rather than the laboratory frame.

Model-Free Aspects – Irreducible Correlation Functions

We have defined the irreducible correlation functions in equation (22), so that using equation (9) the following expression is obtained

$$\begin{aligned} G_m(t) &= \langle D_{0m}^{(2)*}(\Omega_{\mathrm{PL}},0)D_{0m}^{(2)}(\Omega_{\mathrm{PL}},t)\rangle - |\langle D_{0m}^{(2)}(\Omega_{\mathrm{PL}})\rangle|^2 \\ &= [\langle |D_{0m}^{(2)}(\Omega_{\mathrm{PL}})|^2\rangle - |\langle D_{0m}^{(2)}(\Omega_{\mathrm{PL}})\rangle|^2]g_{0m}(t) \\ &= G_m(t=0)g_{0m}(t) \end{aligned} \tag{26}$$

where all symbols have their customary meanings. Here the time-dependent part is factored from the spatial part of the irreducible correlation functions. Use of the closure property leads to $D_{0m}^{(2)}(\Omega_{\mathrm{PL}},t) = \Sigma_n D_{0n}^{(2)}(\Omega_{\mathrm{PD}},t)D_{nm}^{(2)}(\Omega_{\mathrm{DL}})$, so we are able to separate the molecular motion (time dependent) from the static orientation in the frame transformation. For systems with rotational symmetry about a preferred direction (temporal or spatial), the off-diagonal (cross-correlation) terms vanish. Only three different correlation functions are found for the projections of the angular momentum onto the quantization axis (alignment frame or magnetic field direction). (Note that in the case of spherical symmetry, there is no quantization axis for the angular momentum, and so there is only one correlation function for isotropic liquids, e.g., for aqueous protein solutions or detergent micelles.)

In this way, we obtain the irreducible correlation functions within the alignment frame (director ≡ dir in analogy with liquid crystals):

$$\begin{aligned} G_m(t) &= \sum_n [\langle |D_{0n}^{(2)}(\Omega_{\mathrm{PD}})|^2\rangle - |\langle D_{0n}^{(2)}(\Omega_{\mathrm{PD}})\rangle|^2] \\ &\quad \times |D_{nm}^{(2)}(\Omega_{\mathrm{DL}})|^2 g_{0n}(t) \\ &= \sum_n G_n^{\mathrm{dir}}(t)|D_{nm}^{(2)}(\Omega_{\mathrm{DL}})|^2 \end{aligned} \tag{27}$$

The irreducible correlation functions in the preferred alignment system are denoted as follows

$$\begin{aligned} G_n^{\mathrm{dir}}(t) &= [\langle |D_{0n}^{(2)}(\Omega_{\mathrm{PD}})|^2\rangle - |\langle D_{0n}^{(2)}(\Omega_{\mathrm{PD}})\rangle|^2]g_{0n}(t) \\ &= G_n^{\mathrm{dir}}(t=0)g_{0n}(t) \end{aligned} \tag{28}$$

After opening up equation (27), the full expression for the correlation functions in the laboratory frame becomes

$$\begin{aligned} G_m(t) = {} & d_{0m}^{(2)}(\Omega_{\mathrm{DL}})^2 G_0^{\mathrm{dir}}(t) \\ & + [d_{1m}^{(2)}(\Omega_{\mathrm{DL}})^2 + d_{-1m}^{(2)}(\Omega_{\mathrm{DL}})^2]G_1^{\mathrm{dir}}(t) \\ & + [d_{2m}^{(2)}(\Omega_{\mathrm{DL}})^2 + d_{-2m}^{(2)}(\Omega_{\mathrm{DL}})^2]G_2^{\mathrm{dir}}(t) \end{aligned} \tag{29}$$

Note that the laboratory-frame correlation functions are seen to be linear combinations of the correlation functions in the alignment frame.

In what follows, our focus is on the molecular structure and dynamics in the alignment frame. The mean-square amplitudes are summarized by the relations below

$$G_0^{\mathrm{dir}}(t=0) = \langle |D_{00}^{(2)}(\Omega_{\mathrm{PD}})|^2\rangle - |\langle D_{00}^{(2)}(\Omega_{\mathrm{PD}})\rangle|^2 \tag{30}$$

$$G_{\pm 1}^{\mathrm{dir}}(t=0) = \langle |D_{01}^{(2)}(\Omega_{\mathrm{PD}})|^2\rangle \tag{31}$$

$$G_{\pm 2}^{\mathrm{dir}}(t=0) = \langle |D_{02}^{(2)}(\Omega_{\mathrm{PD}})|^2\rangle \tag{32}$$

As discussed above, there are three irreducible correlation functions, because of the axial symmetry of the quadrupolar coupling tensor, together with the rotational symmetry within the alignment frame.

Mean-Square Amplitudes – Clebsch–Gordan Series and Order Parameters

The next step is to evaluate the mean-squared moduli of the Wigner rotation matrix elements $\langle |D_{mn}^{(2)}(\Omega_{\mathrm{PD}})|^2\rangle$, corresponding to the transition matrix elements of the coupling Hamiltonian. Notably, the Wigner rotation matrix elements are the eigenfunctions of the angular momentum operators for a symmetric top,[12,17]

$$\psi_{jmn} = \sqrt{\frac{2j+1}{8\pi^2}}D_{-m-n}^{(j)}(\alpha,\beta,\gamma) \tag{33}$$

In the function space, the symbol Ω denotes the Euler angles (α,β,γ). The Wigner rotation operator considers the effects of three rotation operations expressed by $\widehat{D}(\Omega) = \mathrm{e}^{-i\gamma J_{z''}/\hbar}\,\mathrm{e}^{-i\beta J_{y'}/\hbar}\,\mathrm{e}^{-i\alpha J_z/\hbar}$ where $\{J\}$ denotes the generators of infinitesimal rotations about the various coordinate axes (Figure 2a).[12] The Wigner matrix elements are given by $D_{m'm}^{(j)}(\Omega) = \langle jm'|\widehat{D}^{(j)}(\Omega)|jm\rangle$ in terms of the quantum mechanical (Dirac) bra–ket notation.

We must now calculate the product of two rotation matrix elements, which involves the Clebsch–Gordan coefficients. Because the Wigner rotation matrices are the wavefunctions for the symmetric top, their products represent the coupling

of the associated angular momenta. Hence, we can write the product of two Wigner rotation matrix elements as

$$\begin{aligned} &D^{(j_1)}_{m_1n_1}(\Omega)D^{(j_2)}_{m_2n_2}(\Omega) \\ &= \sum_{J,M,N} \langle j_1j_2m_1m_2|j_1j_2JM\rangle \\ &\times \langle j_1j_2JM|\widehat{D}^{(j_1)}\widehat{D}^{(j_2)}|j_1j_2JN\rangle\langle j_1j_2JN|j_1j_2n_1n_2\rangle \\ &= \sum_{J,M,N} \langle j_1j_2m_1m_2|j_1j_2JM\rangle D^{(J)}_{MN}(\Omega)\langle j_1j_2JN|j_1j_2n_1n_2\rangle \end{aligned} \quad (34)$$

The Clebsch–Gordan coefficients express the unitary transformation either from the uncoupled representation $|j_1j_2m_1m_2\rangle$ to the coupled representation $|j_1j_2JM\rangle$, where $M = m_1 + m_2$, or vice versa from the coupled to the uncoupled representation. In the linear combination, the vector coupling coefficients $\langle j_1j_2m_1m_2|j_1j_2\,JM\rangle$ are the projections of the coupled states onto the uncoupled state, and their squares give the corresponding probabilities. According to group theory, the product representation is reducible, and the representation space splits up into invariant irreducible subspaces, each spanned by only one of the allowed values of J, the total angular momentum. The vector coupling (Clebsch–Gordan) coefficients project out the various irreducible parts of such products. Equation (34) is a coupling rule for the Wigner rotation matrices, and it shows us how the product of two Wigner rotation matrix elements can be expressed in terms of individual matrix elements.

Moreover, Figure 2(b) helps us to understand the evaluation of the Clebsch–Gordan coefficients $\langle j_1j_2JN|j_1j_2n_1n_2\rangle$ that appear in the simplification of Wigner rotation matrix elements of equation (34), as described by Brink and Satchler.[17] According to the semiclassical vector model depicted in Figure 2(b), addition of the individual angular momenta with quantum numbers (j_1, n_1) and (j_2, n_2) yields the coupled state with total quantum numbers (J, N).[17] The evaluation of this coefficient uses the triangle condition $\Delta(j_1j_2J)$ indicated in Figure 2(b), with $|j_1 - j_2| \le J \le j_1 + j_2$ in integer steps for the total angular momentum J. To each value of J, there are $2J + 1$ states with $M = -J, -J+1, \ldots, J$. The additional Clebsch–Gordan coefficients $\langle j_1j_2m_1m_2|j_1j_2JM\rangle$ for the change of basis from the coupled to uncoupled representation are evaluated analogously (see Ref. 17).

To make the calculation simpler and even more convenient, we use $3-j$ symbols in the following expressions, instead of the vector coupling (Clebsch–Gordan) coefficients:

$$\begin{pmatrix} j_1 & j_2 & J \\ m_1 & m_2 & -M \end{pmatrix} \equiv \frac{(-1)^{j_1-j_2+M}}{\sqrt{2J+1}}\langle j_1j_2m_1m_2|j_1j_2JM\rangle \quad (35)$$

Inserting equation (35) in equation (34), we can obtain the values for the mean-squared rotation matrix elements as follows:[7]

$$\begin{aligned} &D^{(j_1)}_{m_1n_1}(\Omega)D^{(j_2)}_{m_2n_2}(\Omega) \\ &= \sum_J (2J+1)\begin{pmatrix} j_1 & j_2 & J \\ m_1 & m_2 & M \end{pmatrix}\begin{pmatrix} j_1 & j_2 & J \\ n_1 & n_2 & N \end{pmatrix} D^{(J)*}_{MN}(\Omega) \end{aligned} \quad (36)$$

Introducing the complex conjugates yields,

$$\begin{aligned} D^{(j_1)*}_{m_1n_1}(\Omega)D^{(j_2)}_{m_2n_2}(\Omega) &= (-1)^{m_1-n_1}\sum_J (2J+1) \\ &\times \begin{pmatrix} j_1 & j_2 & J \\ m_1 & -m_2 & -M \end{pmatrix}\begin{pmatrix} j_1 & j_2 & J \\ n_1 & -n_2 & -N \end{pmatrix} D^{(J)*}_{MN}(\Omega) \end{aligned} \quad (37)$$

In the present case, we consider the squared moduli of the Wigner rotation matrix elements. For simplicity, we assume the alignment frame is coincident with the laboratory frame ($\Omega_{\rm PD} = \Omega_{\rm PL}$). Taking the case of $m = n = 0$ as one example

$$\begin{aligned} |D^{(2)}_{00}(\Omega_{\rm PD})|^2 &= \sum_J (2J+1)\begin{pmatrix} 2 & 2 & J \\ 0 & 0 & 0 \end{pmatrix}\begin{pmatrix} 2 & 2 & J \\ 0 & 0 & 0 \end{pmatrix} D^{(J)*}_{00}(\Omega_{\rm PD}) \\ &= \begin{pmatrix} 2 & 2 & 0 \\ 0 & 0 & 0 \end{pmatrix}^2 d^{(0)}_{00}(\cos\beta_{\rm PD}) + 3\begin{pmatrix} 2 & 2 & 1 \\ 0 & 0 & 0 \end{pmatrix}^2 d^{(1)}_{00}(\cos\beta_{\rm PD}) \\ &+ 5\begin{pmatrix} 2 & 2 & 2 \\ 0 & 0 & 0 \end{pmatrix}^2 d^{(2)}_{00}(\cos\beta_{\rm PD}) + 7\begin{pmatrix} 2 & 2 & 3 \\ 0 & 0 & 0 \end{pmatrix}^2 d^{(3)}_{00}(\cos\beta_{\rm PD}) \\ &+ 9\begin{pmatrix} 2 & 2 & 4 \\ 0 & 0 & 0 \end{pmatrix}^2 d^{(4)}_{00}(\cos\beta_{\rm PD}) \end{aligned} \quad (38)$$

After evaluating the $3-j$ symbols, we obtain the following expression

$$|D^{(2)}_{00}(\Omega_{\rm PD})|^2 = \frac{1}{5} + \frac{2}{7}P_2 + \frac{18}{35}P_4 \quad (39)$$

in terms of $P_j(x)$, the Legendre polynomials where $x \equiv \cos\beta_{\rm PD}$. Here we have used the relations for the rotation matrix elements $D^{(j)}_{mn}(\alpha\beta\gamma) = e^{-im\alpha}d^{(j)}_{mn}(\beta)e^{-in\gamma}$ in which the reduced matrix elements are $d^{(j)}_{00}(\beta) = P_j(\cos\beta)$.

Likewise, we can calculate the values for the other matrix elements. The following expressions for the mean-squared correlation function amplitudes are then obtained:[7]

$$\begin{aligned} G^{\rm dir}_0(t=0) &= \langle|D^{(2)}_{00}(\Omega_{\rm PD})|^2\rangle - |\langle D^{(2)}_{00}(\Omega_{\rm PD})\rangle|^2 \\ &= \frac{1}{5} + \frac{2}{7}\langle P_2\rangle + \frac{18}{35}\langle P_4\rangle - |\langle P_2\rangle|^2 \end{aligned} \quad (40)$$

$$G^{\rm dir}_{\pm1}(t=0) = \langle|D^{(2)}_{01}(\Omega_{\rm PD})|^2\rangle = \frac{1}{5} + \frac{1}{7}\langle P_2\rangle - \frac{12}{35}\langle P_4\rangle \quad (41)$$

$$G^{\rm dir}_{\pm2}(t=0) = \langle|D^{(2)}_{02}(\Omega_{\rm PD})|^2\rangle = \frac{1}{5} - \frac{2}{7}\langle P_2\rangle + \frac{3}{35}\langle P_4\rangle \quad (42)$$

Note that the squared modulus corresponds to $M = N = 0$ in the Clebsch–Gordan series, equation (34). In each case, the mean-square amplitudes depend on both the second- and fourth-rank order parameters $\langle P_2\rangle$ and $\langle P_4\rangle$. For the time-dependent part of the irreducible correlation function, in the data analysis, we consider a stationary Markov process with an exponential time dependence for the correlation functions $g_{0n}(t) = e^{-|t|/\tau_n}$, where the symbol τ_n denotes the correlation time for the nth irreducible component.

Correlation Functions and Spectral Densities – Correlation Times

Recall that Fourier transformation of the irreducible correlation functions yields the corresponding spectral densities. Within the exponentially time-dependent assumption (see above), we shall now see how the spectral densities are expressed:

$$J_n^{\mathrm{dir}}(\omega) = \int_{-\infty}^{\infty} G_n^{\mathrm{dir}}(t)\mathrm{e}^{-i\omega t}\mathrm{d}t = \int_{-\infty}^{\infty} G_n^{\mathrm{dir}}(t=0)\mathrm{e}^{-|t|/\tau_n}\mathrm{e}^{-i\omega t}\mathrm{d}t$$
$$= G_n^{\mathrm{dir}}(0)j_n(\omega) = G_n^{\mathrm{dir}}(0)\frac{2\tau_n}{1+\omega^2\tau_n^2} \qquad (43)$$

Here the spectral densities $j_n(\omega)$ are the Fourier transform partners of the correlation functions $g_n(t) \equiv g_{0n}(t)$ in equation (26). Note that $j_n(\omega)$ and $g_n(t)$ are related to the irreducible spectral densities $J_n(\omega)$ and irreducible correlation functions $G_n(t)$ by the mean-square amplitudes, equations (40)–(42). Evidently it follows that

$$J_1^{\mathrm{dir}}(\omega_0) = G_1^{\mathrm{dir}}(0)\frac{2\tau_1}{1+\omega_0^2\tau_1^2}$$
$$= \left[\frac{1}{5} + \frac{1}{7}\langle P_2\rangle - \frac{12}{35}\langle P_4\rangle\right]\frac{2\tau_1}{1+\omega_0^2\tau_1^2} \qquad (44)$$

$$J_2^{\mathrm{dir}}(2\omega_0) = G_2^{\mathrm{dir}}(0)\frac{2\tau_2}{1+4\omega_0^2\tau_2^2}$$
$$= \left[\frac{1}{5} - \frac{2}{7}\langle P_2\rangle + \frac{3}{35}\langle P_4\rangle\right]\frac{2\tau_2}{1+4\omega_0^2\tau_2^2} \qquad (45)$$

Without any loss of generality, we can consider that the temperature dependence of the correction time for the nucleus of interest is given by $\tau = \tau_0 \mathrm{e}^{E_\mathrm{a}/k_\mathrm{B}T}$, where E_a is the activation barrier. It is possible for E_a to have different values, corresponding to different segments or groups of the molecule. Note that for the limit of $\langle P_2\rangle = \langle P_4\rangle = 1$, only motion about the z-axis of the alignment frame occurs, and thus according to equations (44) and (45), there is no relaxation as expected.

As an example of the GMF analysis, Table 1 provides results for rhodopsin obtained using nonlinear regression fitting of experimental NMR relaxation data.[9] On the basis of experimental measurements of the spin–lattice and quadrupolar-order relaxation rates, with equations (24) and (25), we obtain the experimental spectral densities $J_1(\omega_0)$ and $J_2(2\omega_0)$ in the laboratory frame for various temperatures. The theoretical spectral density expressions using the GMF approach are given by equations (44) and (45), along with the time-dependence assumption of $\tau = \tau_0 \mathrm{e}^{E_\mathrm{a}/k_\mathrm{B}T}$. Using these theoretical formulas, we can then fit the experimental spectral densities, obtaining the values for $G_m(0)$, τ_{0m}, and $E_{\mathrm{a}m}$ where $m = 1, 2$ as summarized in Table 1.

For the case of rhodopsin, the relaxation rates have been measured for nonaligned samples, where the largest peaks correspond to the membrane normal aligned perpendicular to the main magnetic field ($\beta_\mathrm{DL} = \pi/2$). Very little orientation dependence of the relaxation rates is observed within the error of the experimental measurements.[9] One is then justified to assume that the relaxation rates also apply to the parallel orientation ($\beta_\mathrm{DL} = 0$). As mentioned above, $G_1(0)$ and $G_2(0)$ are functions of the moments $\langle P_2\rangle$ and $\langle P_4\rangle$. Knowing the values of $G_1(0)$ and $G_2(0)$ from equations (41) and (42), we can then obtain the values of $\langle P_2\rangle$ and $\langle P_4\rangle$ by the following equations:

$$\langle P_2\rangle = 1 - G_1(0) - 4G_2(0) \qquad (46)$$

$$\langle P_4\rangle = 1 - \frac{5}{3}[2G_1(0) + G_2(0)] \qquad (47)$$

The measured order parameters (moments) can be used to reconstruct the orientational distribution function, even for nonaligned samples.[18] In the present case, we only have relaxation data at a single magnetic field strength, so the data reduction entails comparatively large statistical errors. By combining spin–lattice ($R_{1\mathrm{Z}}$) relation measurements with quadrupolar-order ($R_{1\mathrm{Q}}$) relaxation measurements, and/or by conducting studies at multiple magnetic field strengths, one can determine the order parameters and distribution functions. Lastly, the values of the activation barriers E_{am} reveal how the molecules are activated by external energy fluctuations at a given temperature. We can then compare the results of the activation energies from the GMF method with the values[8,9] previously obtained with a model-dependent treatment, giving close agreement.

Table 1. Parameter values obtained from generalized model-free (GMF) fitting of theoretical spectral densities to experimental ^{2}H NMR relaxation data for rhodopsin[a]

		$G_m(0)^b$	$\tau_{0m}/10^{-12}$ s^b	$E_{am}/10^{-21}$ J
C5-Me	$J_1(\omega_0)$	0.12±0.01	0.72 ± 0.27	15.2 ± 0.8
	$J_2(2\omega_0)$	0.11 ± 0.01	1.35 ± 0.63	14.8 ± 1.0
C9-Me	$J_1(\omega_0)$	—	—	1.73±3.67
	$J_2(2\omega_0)$	—	—	3.31 ± 2.37
C13-Me	$J_1(\omega_0)$	0.048±0.012	0.43±0.17	14.0 ± 1.0
	$J_2(2\omega_0)$	—	—	11.0 ± 1.2

[a]Data from Ref. 8.
[b]Theoretical curves generated from the GMF method fit the data very well; large errors in the fitting parameters occur when the maxima in the plots fall outside the measured range.

Summary of Generalized Model-Free Analysis

In magnetic resonance spectroscopy, the spectral lineshapes and relaxation times depend on the alignment frame of the molecule, together with the symmetries of the Wigner rotation matrix elements, the mean-square amplitudes, and the associated correlation times. Through a connection to angular momentum theory, we are able to apply the powerful theorems of group theory to (bio)molecular dynamics in a model-free way. GMF analysis is based on an irreducible representation of the nuclear spin Hamiltonian, with a change of basis from the more usual Cartesian basis to a spherical basis. Dynamics are considered to be represented by a stationary Markov process.

The main additional assumption is the point group symmetry of the molecule or phase of interest. The essential features are (i) an irreducible representation of the spin couplings and frame transformations using the Wigner rotation matrix; (ii) the use of closure to expand or suppress intermediate frame transformations; and (iii) the use of the Clebsch–Gordan series expansion to evaluate the mean-square amplitudes or moments of the orientational distribution function. The mean-squared amplitudes obtained from the order parameters or moments of the spectral lineshapes tell us about the averaged structures. Conversely, the spectral densities of motion and the correlation times reveal the molecular dynamics. For the specific case of solid-state NMR, motional information is obtained from the mean-square amplitudes and the motional rates of fast local motions, without any consideration of slower (global) motions of the system. By induction, the same type of treatment can be applied for global motions, yielding isomorphous theoretical expressions for the experimental observables. The GMF method shown here is simple and general, and has great potential to be used as a guide or introduction to more detailed theories.[19–21]

Extension to Multi-Scale Motions

The advantage of a representation using irreducible tensor operators is that multiple coordinate transformations can be handled readily (see Figure 3 as one example). At a model-free level, one can then introduce the mathematical isomorphism of the various coupling Hamiltonians to obtain results for multiple motions, with different amplitudes and time scales. Referring back to Figure 4, we can see that the RQCs are manifested by the spectral lineshapes, and can include contributions from the various types of motions. Model-free aspects are pertinent to a multiscale formulation of the dynamics by introducing fast motions due to modulation of a static coupling tensor. Slower motions modulate the residual coupling tensor $\langle V_m^{(2)} \rangle$, i.e., remaining after pre-averaging over the spatial coordinates due to fast internal motions. Statistical independence of the relatively fast and slow fluctuations is assumed, meaning that the mode coupling is neglected as a first approximation.[6] The GMF method considers the anisotropic alignment axis, and comes up with mean-squared amplitudes for motions with different time scales, as well as the distribution of correlation times.

Although we have only presented the effects of fast motions on the static coupling, the treatment of slow motions with larger amplitude is straightforward. It involves the residual couplings $\langle \chi_Q \rangle \sim \langle V_0^{(2)} \rangle$ remaining after pre-averaging due to faster local motions. Fluctuations of $\langle V_0^{(2)} \rangle$ can occur with respect to the spatial average over both the fast and slow motions $\sim \langle V_0^{(2)\mathrm{lab}} \rangle$. Recognizing the mathematical isomorphism of the static and residual coupling tensors, we find that the relatively slow motions have the same form as we derived earlier for the fast motions. By simply substituting the residual coupling constants $\{\langle \chi_Q \rangle, \langle \eta_Q \rangle\}$ for the static values $\{\chi_Q, \eta_Q\}$, we obtain the corresponding relaxation rate formulas.[6] For the example of rhodopsin presented here, our consideration of only fast methyl group motions in the theoretical fitting agrees very well with experimental measurements. However, in other cases such as membrane lipids, consideration of collective slow motions is necessary to explain the experimental NMR relaxation data.[22]

Comparison with Other Treatments

The GMF approach was introduced in 1982 by Brown simultaneously with the more well-known Lipari–Szabo model-free (MF) approach,[6,19] which is applicable to proteins in solution with overall tumbling motions. By contrast, in the GMF method, a preferred alignment frame is considered, together with the mean-squared amplitudes and rates of the fluctuations. For biomembranes, the sample is often in a liquid-crystalline state, and overall motions are restricted in their amplitudes, instead of being isotropic. In the limit of orientational averaging, the independently obtained result of Giovanni Lipari and Attila Szabo is immediately obtained.[6] When an ordering potential is absent, the GMF approach also yields Woessner's classical results for isotropic reorientation[23] as the limit.[6] Neither the GMF nor MF approach considers mode coupling (cross correlations) of the various irreducible components with different stochastic amplitudes – statistical independence is assumed as a first approximation. For insightful discussions of more detailed models, including mode coupling, see the papers of Bertil Halle[20] and Eva Meirovitch and Jack Freed *et al.*[21] Cross-correlation terms between fast local motions and relatively slow overall motions enable more detailed results to be obtained as compared with model-free treatments. The approaches have varying levels of detail – considered together, they offer the potential for insight into fluctuations of (bio)molecules in relation to their properties.

Application to Rhodopsin

As an illustration, we have applied the GMF method to the reduction of experimental NMR relaxation data to investigate the structure, dynamics, and function of rhodopsin. The visual protein is a prototypical G-protein-coupled receptor (GPCR), and its 3-D structure is known from X-ray crystallography (Figure 3b).[24,25] In the dark state, rhodopsin is stabilized by its cofactor retinal acting as an inverse agonist.[25] Light-induced 11-*cis* to all-*trans* isomerization of retinal yields less stable intermediates (Meta I and Meta II), that give activating conformational fluctuations of the protein. To study rhodopsin activation, both structural and dynamical information is necessary, for which solid-state NMR spectroscopy can play an important role.[9] The rotational dynamics for three key methyl positions of the retinal cofactor bound to rhodopsin have been studied in experimental work (Figure 4a). Application of GMF analysis can guide more specific formulations of analytical models in closed form, or aid the development of the force fields in numerical MD simulations.

Solid-state ^{2}H NMR relaxation gives a unique, site-directed approach to study the local dynamics of retinal within the ligand-binding pocket of the photoreceptor.[8] Representative experimental data for rhodopsin are included in Figure 5(a) and (b), which show the partially-relaxed ^{2}H NMR spectra obtained with an inversion-recovery pulse sequence (180°-τ-acquire) as a function of the delay (τ). Figure 5(c)

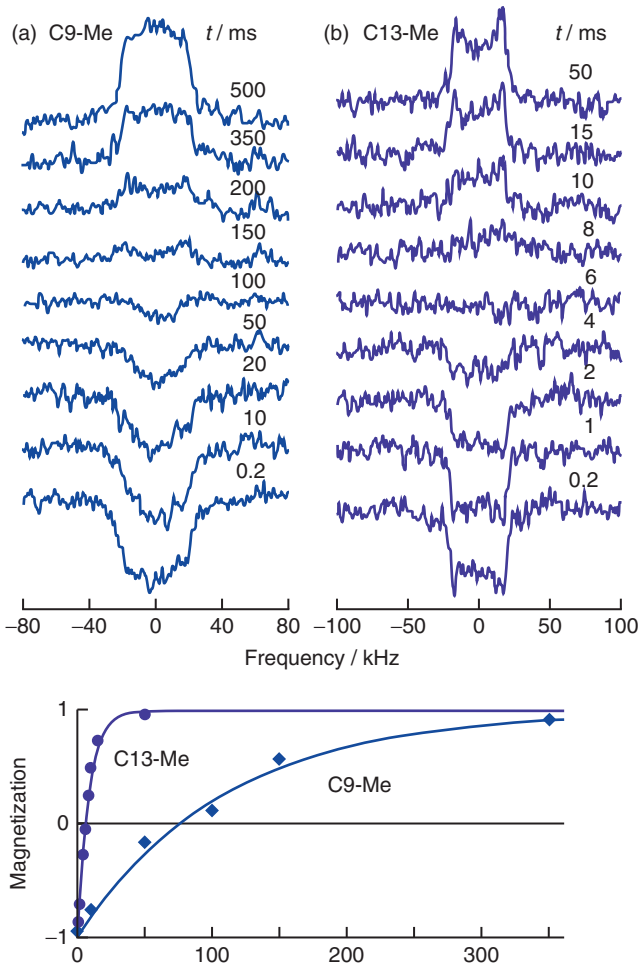

Figure 5. Illustration of experimental measurement of spin–lattice (T_{1Z}) relaxation times using inversion-recovery pulse sequence. (a,b) Partially relaxed solid-state ^{2}H NMR spectra for the C9- and C13-methyl groups of retinal cofactor bound to rhodopsin embedded in lipid bilayer membranes. The 180° pulse inverts the direction of the C9-Me or C13-Me magnetization. The partially relaxed spectra acquired with a quadrupolar-echo pulse sequence at different time intervals show recovery of the equilibrium magnetization. (c) Nonlinear regression fitting of the spectral magnetization as a function of time allows determination of the spin–lattice relaxation time (T_{1Z}). (Adapted from Ref. 8. © Nature Publishing Group, 2011)

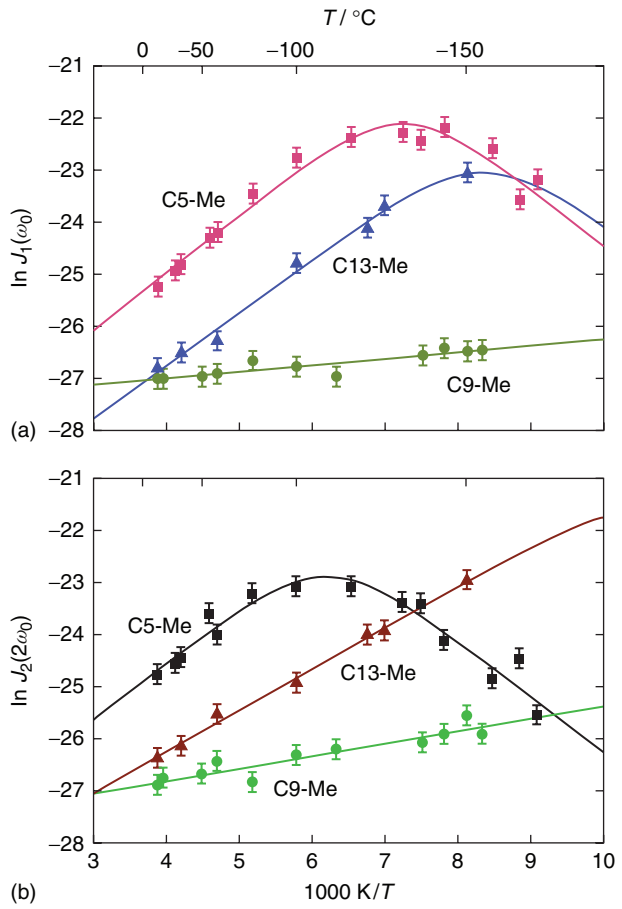

Figure 6. Generalized model-free (GMF) analysis of individual spectral densities of motion describes methyl group dynamics of the retinal cofactor of rhodopsin. (a, b) Plots of irreducible spectral densities $J_1(\omega_0)$ and $J_2(2\omega_0)$ versus inverse temperature indicate matching of the stochastic fluctuations to the nuclear Larmor frequency (ω_0). The spectral densities show a distinct maximum that depends on the ^{2}H-labeled methyl position of retinal. Slower motions have optimal matching (maximum) at a higher temperature, and vice versa. The width of the plots depends oppositely on the potential barrier for the methyl rotation. The maxima occur in the order: C5-Me > C13-Me > C9-Me for both the $J_1(\omega_0)$ and $J_2(2\omega_0)$ spectral densities. The width of the spectral density plots follows the opposite trend: C5-Me < C13-Me < C9-Me. Note that the mobility of the C9-Me group is greatest, followed by the C13-Me group and the C5-Me group of the β-ionone ring of retinal

shows nonlinear regression fits of the inversion-recovery curves, from which the spin–lattice relaxation times (T_{1Z}) are extracted. Additional experiments have determined ^{2}H NMR relaxation times (T_{1Q}) for the decay of quadrupolar order (see Biosynthesis and Metabolic Pathways: Carbon-13 and Nitrogen-15 NMR, Biosynthesis and Metabolic Pathways: Deuterium NMR, Protein Dynamics from NMR Relaxation, and Protein Dynamics from Solid State NMR). Using the GMF method, we succeeded in disentangling the experimental relaxation rates, and in representing them by the irreducible spectral densities of motion, see equations (24) and (25) (Figure 6). Notably, our NMR experimental results indicate the presence of site-specific differences in the internal dynamics of retinal. For the spectral density plot for $J_1(\omega_0)$ in Figure 6(a), we observe distinct maxima for the C5- and C13-methyl groups, but not for the C9-methyl position. Analogous behavior is seen for the $J_2(2\omega_0)$ spectral density in Figure 6(b). Such maxima imply an optimal matching between the spectral density of the molecular fluctuations and the energy gap for the nuclear spin transitions. At the maximum point, an effective correlation time $\tau_c \approx 1/\omega_0$ characterizes the motions at the corresponding temperature. Displacement of the minimum to lower temperature corresponds to faster motions, and vice versa. According to the GMF analysis in Figure 6, for rhodopsin, the C9-methyl group dynamics are fastest, followed by the C13- and C5-methyl groups in that order. Additional changes are observed in the site-specific methyl dynamics of retinal upon light activation of rhodopsin

(not shown).[8] Results of the GMF method can then be used in MD simulations to improve the validity of the force fields for rhodopsin and other retinal proteins.[26,27]

Conclusions and Future Outlook

The simplicity of the GMF analysis method establishes its potential wide applicability in physical chemistry and molecular biophysics. The GMF approach can be implemented with regard to aligned biopolymers including fibrous proteins and nucleic acids, as well as proteolipid membranes. In the case of proteins that are neither crystalline nor solubilized in aqueous media, it allows the investigation of their structure, dynamics, and function. Moreover, the GMF analysis helps to shape our understanding of the role of conformational fluctuations in biophysical mechanisms involving both proteins and lipids. Such knowledge opens new windows to understand the functional dynamics of biomolecules, going beyond the static view of X-ray crystallography to a dynamic vision of structure based on NMR spectroscopy.

Acknowledgments

Research was sponsored by the US National Institutes of Health and by the Arizona Biomedical Research Commission. We thank O. L. A. Monti, R. W. Pastor, A. Sanov, and A. Szabo for informative discussions.

Biographical Sketches

Xiaolin Xu. *b* 1987. BS, 2011, Henan University at Henan, China. Currently PhD student in Department of Physics, University of Arizona, USA. Research specialties: theoretical and mathematical physics; application of solid-state ^{2}H NMR spectroscopy to studies of phospholipid bilayers and membrane proteins; protein structural and dynamical studies.

Andrey V. Struts. *b* 1959. MSc, 1982, Leningrad State University, Russia, PhD, 1991, St. Petersburg State University, Russia. Engineer, 1982–1987, Junior Research Associate, 1987–1992, Research Associate, 1992–1995, Senior Scientist, 1996–2010, St. Petersburg State University, Russia. Government of Italy Postdoctoral Fellow, University of Pisa, Italy, 1996. Research Associate, 2001–2009, Research Scientist, 2009–2010, University of Arizona, USA. Head of Medical Physics Division, 2011–2013, Associate Professor of Physics, St. Petersburg State Medical University, Russia, 2014-present. Approx. 50 publications. Research specialties: application of nuclear magnetic resonance spectroscopy to molecular structure and dynamics in orientationally disordered crystals, liquid crystals, membranes, and membrane proteins.

Michael F. Brown. *b* 1948. AB, 1970, University of California at Santa Cruz, USA, PhD, 1975, University of California at Santa Cruz. NIH Postdoctoral Fellow, University of Basel, Switzerland, and Max-Planck-Institute for Medical Research, Heidelberg, Germany, 1976–1979. NIH Postdoctoral Fellow, University of California at Berkeley, USA, 1979–1980. Assistant Professor of Chemistry, 1980–1985, Associate Professor of Chemistry, 1985–1987, University of Virginia, USA. Professor of Chemistry, 1987-present, Professor of Physics, University of Arizona, USA, 2003-present. Approx. 140 publications. Research specialties: the theory and application of nuclear spin relaxation to liquid-crystalline materials; applications of NMR to lipid bilayers and proteins; structure and dynamics of proteins, biophysical chemistry of membranes; molecular basis of vision.

Related Articles

Protein Dynamics by NMR Spin Relaxation: The Slowly Relaxing Local Structure Perspective; Bilayer Membranes: Deuterium and Carbon-13 NMR; Amphiphilic Liquid Crystalline Samples: Nuclear Spin Relaxation; Deuteron Relaxation Rates in Liquid Crystalline Samples: Experimental Methods; Liquid Crystalline Samples: Relaxation Mechanisms; Relaxation Studies of Solid Biopolymers; Internal Spin Interactions and Rotations in Solids; Membranes: Deuterium NMR; Average Hamiltonian Theory; Brownian Motion and Correlation Times; Relaxation Theory: Density Matrix Formulation; Relaxation Theory for Quadrupolar Nuclei; Biosynthesis and Metabolic Pathways: Carbon-13 and Nitrogen-15 NMR; Biosynthesis and Metabolic Pathways: Deuterium NMR; Protein Dynamics from NMR Relaxation; Protein Dynamics from Solid State NMR

References

1. U. Häberlen, High Resolution NMR in Solids: Selective Averaging, Academic Press: New York, 1976.
2. H. W. Spiess, in NMR Basic Principles and Progress, eds P. Diehl, E. Fluck, and R. Kosfeld, Springer-Verlag: Heidelberg, 1978, Vol. 15, p. 55.
3. M. F. Brown, in Biological Membranes: A Molecular Perspective from Computation and Experiment, eds K. M. Merz Jr and B. Roux, Birkhäuser: Basel, 1996, p. 175.
4. C. P. Slichter, Principles of Magnetic Resonance, 3rd edn, Springer-Verlag: Heidelberg, 1990.
5. M. F. Brown, J. Seelig, and U. Häberlen, *J. Chem. Phys.*, 1979, **70**, 5045.
6. M. F. Brown, *J. Chem. Phys.*, 1982, **77**, 1576.
7. T. P. Trouard, T. M. Alam, and M. F. Brown, *J. Chem. Phys.*, 1994, **101**, 5229.
8. A. V. Struts, G. F. J. Salgado, K. Martínez-Mayorga, and M. F. Brown, *Nat. Struct. Mol. Biol.*, 2011, **18**, 392.
9. A. V. Struts, G. F. J. Salgado, and M. F. Brown, *Proc. Natl. Acad. Sci. U. S. A.*, 2011, **108**, 8263.
10. J. J. Sakurai and J. Napolitano, Modern Quantum Mechanics, 2nd edn, Addison-Wesley: San Francisco, 2010.
11. M. F. Brown and S. I. Chan, in Encyclopedia of Nuclear Magnetic Resonance, eds D. M. Grant and R. K. Harris, Wiley: New York, 1996, Vol. 2, p. 871.
12. M. E. Rose, Elementary Theory of Angular Momentum, Wiley: New York, 1957.
13. A. Abragam, The Principles of Nuclear Magnetism, Oxford University Press: London, 1961.
14. M. H. Levitt, Spin Dynamics: Basics of Nuclear Magnetic Resonance, Wiley: Chichester, 2001.
15. A. V. Struts, G. F. J. Salgado, K. Tanaka, S. Krane, K. Nakanishi, and M. F. Brown, *J. Mol. Biol.*, 2007, **372**, 50.
16. A. G. Redfield, *Adv. Magn. Reson.*, 1965, **1**, 1.
17. D. M. Brink and G. R. Satchler, Angular Momentum, Oxford University Press: London, 1968.
18. H. I. Petrache, S. W. Dodd, and M. F. Brown, *Biophys. J.*, 2000, **79**, 3172.
19. G. Lipari and A. Szabo, *J. Am. Chem. Soc.*, 1982, **104**, 4546.
20. B. Halle, *J. Chem. Phys.*, 2009, **131**, 224507.
21. E. Meirovitch, Y. E. Shapiro, A. Polimeno, and J. H. Freed, *J. Phys. Chem. A*, 2006, **110**, 8366.

22. G. V. Martinez, E. M. Dykstra, S. Lope-Piedrafita, C. Job, and M. F. Brown, *Phys. Rev. E*, 2002, **66**, 050902.
23. D. E. Woessner, *J. Chem. Phys.*, 1962, **36**, 1.
24. J. Li, P. C. Edwards, M. Burghammer, C. Villa, and G. F. X. Schertler, *J. Mol. Biol.*, 2004, **343**, 1409.
25. S. O. Smith, *Ann. Rev. Biophys.*, 2010, **39**, 309.
26. B. Mertz, A. V. Struts, S. E. Feller, and M. F. Brown, *Biochim. Biophys. Acta*, 2012, **1818**, 241.
27. S. Zhu, M. F. Brown, and S. E. Feller, *J. Am. Chem. Soc.*, 2013, **135**, 9391.